Outer membrane vesicles catabolize lignin-derived aromatic compounds in *Pseudomonas putida* KT2440

Davinia Salvachúa[a,b,1], Allison Z. Werner[a,b,1], Isabel Pardo[a,1], Martyna Michalska[c,1], Brenna A. Black[d], Bryon S. Donohoe[d], Stefan J. Haugen[d], Rui Katahira[a], Sandra Notonier[a,b], Kelsey J. Ramirez[d], Antonella Amore[d], Samuel O. Purvine[e], Erika M. Zink[e], Paul E. Abraham[b,f], Richard J. Giannone[b,f], Suresh Poudel[b,f], Philip D. Laible[c], Robert L. Hettich[b,f,2], and Gregg T. Beckham[a,b,2]

[a]National Bioenergy Center, National Renewable Energy Laboratory, Golden, CO 80401; [b]Center Bioenergy Innovation, Oak Ridge National Laboratory, Oak Ridge, TN 37830; [c]Biosciences Division, Argonne National Laboratory, Lemont, IL 60439; [d]Biosciences Center, National Renewable Energy Laboratory, Golden, CO 80401; [e]Environmental Molecular Sciences Laboratory, Pacific Northwest National Laboratory, Richland, WA 99352; and [f]Chemical Sciences Division, Oak Ridge National Laboratory, TN 37830

Edited by Alexis T. Bell, University of California, Berkeley, CA, and approved February 27, 2020 (received for review December 1, 2019)

Lignin is an abundant and recalcitrant component of plant cell walls. While lignin degradation in nature is typically attributed to fungi, growing evidence suggests that bacteria also catabolize this complex biopolymer. However, the spatiotemporal mechanisms for lignin catabolism remain unclear. Improved understanding of this biological process would aid in our collective knowledge of both carbon cycling and microbial strategies to valorize lignin to value-added compounds. Here, we examine lignin modifications and the exoproteome of three aromatic–catabolic bacteria: *Pseudomonas putida* KT2440, *Rhodoccocus jostii* RHA1, and *Amycolatopsis* sp. ATCC 39116. *P. putida* cultivation in lignin-rich media is characterized by an abundant exoproteome that is dynamically and selectively packaged into outer membrane vesicles (OMVs). Interestingly, many enzymes known to exhibit activity toward lignin-derived aromatic compounds are enriched in OMVs from early to late stationary phase, corresponding to the shift from bioavailable carbon to oligomeric lignin as a carbon source. In vivo and in vitro experiments demonstrate that enzymes contained in the OMVs are active and catabolize aromatic compounds. Taken together, this work supports OMV-mediated catabolism of lignin-derived aromatic compounds as an extracellular strategy for nutrient acquisition by soil bacteria and suggests that OMVs could potentially be useful tools for synthetic biology and biotechnological applications.

extracellular vesicle | lignin valorization | outer membrane vesicle | *Pseudomonas putida* | biological funneling

Plant cell walls are a complex matrix of biopolymers that are highly recalcitrant to decay, mainly due to the presence of lignin (1), which is an aromatic polymer synthesized via radical coupling of monolignols (2). Given its prevalence in plants, lignin is estimated to account for 30% of Earth's nonfossil organic carbon (2). Despite the natural abundance of lignin, relatively few microbes can efficiently breakdown this biopolymer, and for many years, oxidoreductases, such as laccases and peroxidases, secreted by white rot fungi were thought to be the major enzymatic actors in biological lignin depolymerization (3). However, recent work has begun to suggest an important role for bacteria in lignin conversion (4–7).

The liberated products of lignin depolymerization represent a large carbon and energy source for microbial life. To understand the fate of these compounds, the environmental microbiology community has mapped various pathways that microbes use for the intracellular catabolism of monomeric aromatic species, motivated in part by the release of xenobiotic aromatic pollutants (8). These efforts have led to deeper understanding of the primary pathways for bacterial catabolism of lignin-derived monomeric aromatic compounds (5, 6). Pioneering research, mainly from Masai and coworkers (4, 6), has also led to the discovery of multiple bacterial pathways for the cleavage of lignin-derived dimers (5). Taken together, these studies have gained the attention of the biomass conversion research community, wherein lignin conversion to valuable products is recognized as a critical need for a successful plant-based carbon economy (9–12).

Since large lignin oligomers, especially with carboxylate groups or covalently linked glucosides, may not readily translocate across the bacterial cell membrane (13), it is commonly assumed that secreted enzymes are responsible for the extracellular depolymerization or modification of lignin. Exoproteomics studies have been conducted in a few aromatic–catabolic bacteria to investigate microbe–lignin interactions (14–16). However, these studies are few and typically do not consider spatiotemporal changes in the extracellular milieu or the compartmentalization of various biological functions. Overall, improved understanding about how

Significance

The valorization of the plant polymer lignin is critical to enable the bioeconomy, but the heterogeneity of lignin presents a barrier to its use. Natural microbial conversion processes funnel aromatic compound mixtures to single products and thus, have emerged as a means to overcome lignin heterogeneity. Accordingly, understanding the mechanisms that bacteria use to convert lignin degradation products is of importance for their eventual industrial application. Here, we demonstrate that a promising bacterial chassis for lignin-relevant synthetic biology, *Pseudomonas putida*, secretes outer membrane vesicles that turn over aromatic compounds extracellularly. From this work, we propose a mechanism for extracellular nutrient acquisition from aromatic compounds by soil bacteria, which holds promise for improving the efficiency of microbial lignin conversion.

Author contributions: D.S., A.Z.W., I.P., M.M., B.S.D., P.E.A., R.J.G., P.D.L., R.L.H., and G.T.B. designed research; D.S., A.Z.W., I.P., M.M., B.A.B., B.S.D., S.J.H., R.K., S.N., K.J.R., A.A., S.O.P., E.M.Z., P.E.A., R.J.G., and S.P. performed research; D.S., A.Z.W., I.P., M.M., B.S.D., R.K., K.J.R., A.A., S.O.P., P.E.A., R.J.G., S.P., P.D.L., R.L.H., and G.T.B. analyzed data; and D.S., A.Z.W., I.P., and G.T.B. wrote the paper.

The authors declare no competing interest.

This article is a PNAS Direct Submission.

Data deposition: The proteomics data from *Pseudomonas putida*, *Rhodoccocus jostii*, and *Amycolatopsis* sp. have been deposited in the MassIVE database (accession no. MSV000084524) and the ProteomeXchange database (accession no. PXD016114). The proteomics data from *P. putida* OMV and VFS are available at the MassIVE database (accession no. MSV000084506).

[1]D.S., A.Z.W., I.P., and M.M. contributed equally to this work.

[2]To whom correspondence may be addressed. Email: gregg.beckham@nrel.gov or hettichrl@ornl.gov.

This article contains supporting information online at https://www.pnas.org/lookup/suppl/doi:10.1073/pnas.1921073117/-/DCSupplemental.

First published April 3, 2020.

microbes interact with lignin and lignin-derived compounds in the extracellular milieu would provide further insights into global carbon cycling and biological strategies to valorize lignin.

To that end, here we study the spatiotemporal interaction of three soil bacteria (*Pseudomonas putida* KT2440, *Rhodococcus jostii* RHA1, and *Amycolatopsis* sp. American Type Culture Collection [ATCC] strain 39116) with a lignin-rich substrate via nuclear magnetic resonance (NMR) spectroscopy to track the lignin chemistry as a function of microbial cultivations and exoproteomics to identify the proteins in the extracellular environment. In all three bacteria, the exoproteomes are distinct from the proteins detected in the intracellular fractions. However, the *P. putida* lignin-induced exoproteome is highly abundant and dynamic in its protein content compared with the other organisms. This bacterium is also characterized by the abundant secretion of outer membrane vesicles (OMVs) in the presence of lignin, which are known to be implicated in a diverse set of functional roles in gram-negative (17) [and some gram-positive (18)] bacteria, including communication, virulence, and nutrient acquisition, among others (19, 20). We conduct further proteomics experiments, which demonstrate that these OMVs dynamically encapsulate enzymes, including those in the β-ketoadipate (βKA) pathway [a central pathway to the catabolism of lignin-derived aromatics in this microbe (21)]. In addition, functional assays demonstrate that isolated OMVs are involved in 4-hydroxybenzoate (4-HBA) and protocatechuate (PCA) turnover, key compounds in aromatic catabolism through the βKA pathway. Overall, this work presents a role for OMVs in the extracellular catabolism of lignin-derived compounds by a soil microbe. The capability OMV secretion for extracellular catabolism of toxic substrates may be an additional reason that *P. putida* KT2440 is inherently such a robust bacterium (22). We also discuss the ability to harness OMVs as a general means to conduct enzymatic reactions extracellularly (for example, to consume or produce toxic compounds) for synthetic biology applications.

Results

To explore the interaction of aromatic–catabolic bacteria with lignin, we selected a gram-negative bacterium (*P. putida* KT2440; hereafter, *P. putida*) and two gram-positive bacteria (*R. jostii* RHA1 and *Amycolatopsis* sp. ATCC 39116; hereafter, *R. jostii* and *Amycolatopsis* sp.), which we previously reported to utilize a significant amount of lignin in a soluble, lignin-rich stream compared with other aromatic–catabolic bacteria (7). The lignin-rich substrate utilized in this study is a soluble alkaline extract from corn stover, which contains aromatic monomers and oligomers (*SI Appendix*, Fig. S1) that retain β-O-4 linkages from native lignin.

We first analyzed bacterial growth and carbon utilization in lignin-rich media (i.e., aromatic compounds, carboxylic acids, and supplemental glucose) and for comparison purposes, also in lignin-free media (containing glucose as the only carbon and energy source) over 120 h. Utilizable aromatic monomers, aliphatic carboxylic acids, and glucose were depleted within 24 h in *P. putida* cultures and within 72 h in *R. jostii* and *Amycolatopsis* sp. (Fig. 1 *A*–*C* and *SI Appendix*, Fig. S2), with oligomeric lignin as the primary remaining carbon source. The initial lignin content (monomeric + oligomeric) in these cultures was 1.7 g/L, and the total concentration of monomeric aromatic compounds was 0.27 g/L (16% of the total lignin) (*SI Appendix*, Table S1). Since these organisms utilized lignin contents of 23.4, 18.9, and 24.4% (Fig. 1 *A*–*C*) as measured with our previous approach (7), it is likely that they utilized a small fraction of lignin oligomers (7.4 ± 2.1% for *P. putida*, 2.9 ± 2.3% for *R. jostii*, and 8.4 ± 0.2% for *Amycolatopsis* sp. by 120 h).

To understand the chemical changes in lignin, we also conducted two-dimensional (2D) heteronuclear single-quantum correlation (HSQC) NMR spectroscopy as a function of time (Fig. 1 *D*–*H* and *SI Appendix*, Figs. S3–S6). This technique is commonly used to understand lignin chemistry (23, 24), including to elucidate modifications by chemical catalysts (25) and ligninolytic enzymes (26, 27). The major changes occurred from 0 to 72 h. Ferulic acid (FA) and *p*-coumaric acid (*p*CA)-derived signals such as FA_2, pCA_β, $pCA_{2/6}$, and pCA_α + FA_α disappear at 72 h in *P. putida* and *R. jostii* treatments, which corresponds to *p*CA and FA depletion analyzed by liquid chromatography (LC) mass spectrometry (MS/MS) (*SI Appendix*, Fig. S2). Conversely, *Amycolatopsis* sp. still exhibits signals for FA_2 and pCA_α + FA_α at 120 h, although the latter was reduced compared with the noninoculated control. 2D-HSQC-NMR spectra also exhibit a reduction in the A_α and A_β signals from the β-O-4 bond in the three bacteria compared with the control, which suggests that these bacteria are breaking down oligomeric lignin. However, it is worth noting that this cleavage does not necessarily imply increased lignin utilization.

To provide insights into the extracellular enzymes potentially involved in lignin catabolism, we conducted differential (lignin-free and lignin-rich media), spatial (intracellular and extracellular), and temporal (24, 72, and 120 h of incubation) proteomic analyses with the three bacteria (Dataset S1). *P. putida* reached stationary phase at 24 h, and *R. jostii* and *Amycolatopsis* sp. reached stationary phase between 48 and 72 h, when most of the readily available carbon sources were depleted (Fig. 1 *A*–*C*). Despite reaching stationary phase—a growth phase that leads to cell lysis events—the percentages of differential proteins between the extracellular and intracellular fractions were 54, 33, and 60% in *P. putida*, *R. jostii*, and *Amycolatopsis* sp., respectively (*SI Appendix*, Fig. S7), indicating that the intracellular and extracellular fractions are different. The extracellular fraction contained a less diverse set of proteins compared with the intracellular fraction in all cases, and *P. putida* exhibited the highest number of lignin-induced extracellular proteins compared with both the intracellular fraction and the other organisms (Fig. 1 *I*–*K* and *SI Appendix*, Fig. S8). It is notable that the other microbes exhibit a higher number of predicted proteins from the genome than *P. putida* (*SI Appendix*, Table S2). Furthermore, the *P. putida* exoproteome showed that a higher number of proteins were enriched when oligomeric lignin became the major carbon source (from 24 to 72 h) compared with the other two organisms (from 72 to 120 h) (Fig. 1 *I*–*K*).

To identify putative enzymes that could be involved in lignin modification and/or depolymerization from these large pools of proteins, here we focused on lignin-induced extracellular proteins that were not detected in the intracellular compartment (*SI Appendix*, Fig. S9). The most represented catalytic functions, according to gene ontology annotation, were hydrolases and oxidoreductases in the three organisms (~30 to 40%) (*SI Appendix*, Tables S3–S5). Notably, these functions were further enriched in the subset of proteins that appeared or increased at the time at which oligomeric lignin was the major carbon source—up to 56% in *P. putida* and 80% in *Amycolatopsis* sp. (the percentages remained similar in *R. jostii*, ~40%) (*SI Appendix*, Tables S6–S8). Most of the lignin-depolymerizing enzymes described to date, including some potentially involved in β-O-4 cleavage [i.e., dye decolorizing peroxidases (DyPs) (28–30), multicopper oxidases (31, 32)], belong to the broad group of oxidoreductases. In the current analysis, we have only detected a DyP in *P. putida*. However, we also found other enzymes that could be potentially involved in the modification of both oligomeric and monomeric aromatic or phenolic compounds (*SI Appendix*, Tables S3–S8). For instance, azoreductases (33, 34), a xenobiotic reductase (35), and a 2,3-quercetin dioxygenase (36) were detected in *P. putida*. All but DyP appeared or were enriched when oligomeric lignin was the major carbon source. In the case of *R. jostii*, a cholesterol oxidase (37) and a cytochrome P450 (38) were also observed. In *Amycolatopsis* sp., another cholesterol oxidase, cytochrome P450, and two oxidoreductases (one potentially belonging to the glucose–methanol–choline superfamily) (39) were detected. Among these enzymes, only the cytochrome P450 in *R. jostii* and cholesterol oxidase in

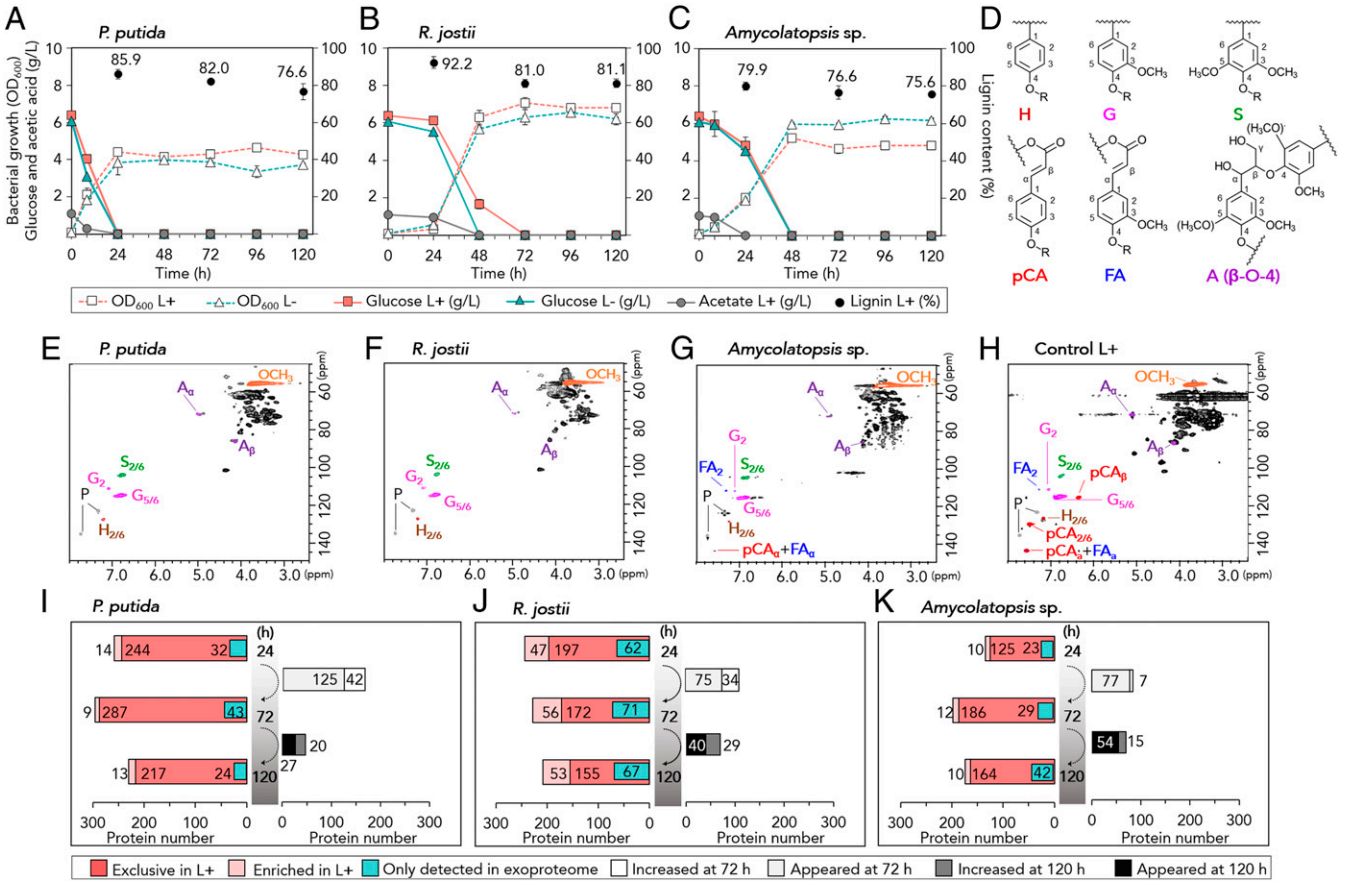

Fig. 1. Chemical and proteomics analyses in lignin-free (L–) and lignin-rich (L+) bacterial cultures. (*A–C*) Bacterial growth (OD_{600}) and concentrations of the major carbon sources in (*A*) *P. putida*, (*B*) *R. jostii*, and (*C*) *Amycolatopsis* sp. cultivations. The concentrations of minor carbon sources are shown in *SI Appendix*, Fig. S2. Error bars show the absolute difference between two biological replicates. (*D*) Schematic representation of atom signals identified by 2D-HSQC-NMR. (*E–H*) Structural lignin units analyzed by 2D-HSQC-NMR spectroscopy in 5-d L+ cultures of (*E*) *P. putida*, (*F*) *R. jostii*, (*G*) *Amycolatopsis* sp., and (*H*) noninoculated 5-d sample (control). Temporal and high-resolution spectra of the side chain and aromatic regions are presented in *SI Appendix*, Figs. S3–S6. OCH_3, methoxy groups; *P*, pyridine (internal standard). (*I–K*) Results from proteomic analyses in (*I*) *P. putida*, (*J*) *R. jostii*, and (*K*) *Amycolatopsis* sp. cultures. The left side of the bar chart shows the number of exclusive (in red) and enriched (in pink) proteins in L+ cultures compared with L– cultures as well as the number of proteins from that pool of proteins that appear only in the exoproteome compared with the intracellular fraction (in blue). The right side of the bar chart shows the number of proteins that appear or increase over time (from 24 to 72 h or from 72 to 120 h) within the pool of exclusive or enriched proteins in L+ cultures. The complete list of proteins is shown in *SI Appendix*, Tables S3–S8. These analyses originate from two biological replicates and two technical replicates in each organism, each time point (24, 72, 120 h), each media (L+, L–), and each protein location (extracellular vs. intracellular). Proteins in L+ cultures with absolute log ratios value that exceeded 2 SDs of all log ratios within the pairwise comparison L+ vs. L– are denoted as "enriched." Proteins in 72- or 120-h cultures with absolute log ratios value that exceeded 2 SDs of all log ratios within the pairwise comparison 72 vs. 24 h or 120 vs. 72 h, respectively, are denoted as "increased."

Amycolatopsis sp. appeared from 72 and 120 h, when oligomeric lignin is the major remaining carbon source (protein access numbers are in *SI Appendix*, Tables S3–S8). Additional information on these oxidoreductases as well as other enzymes that were not part of this protein subset and that are potentially involved in lignin modification is presented in *SI Appendix*, *Text* S1.

A question that arises from these data is how the various proteins are transported from the cell to the extracellular milieu. We used several algorithms (i.e., SignalP, TatP, SecP, PSORTb) to predict protein location or export from the cytoplasm (40–43). Only 40% of the lignin-induced proteins (that were exclusively detected in the extracellular fraction) were predicted to be extracellular and/or exported in *P. putida* by at least one of the algorithms, whereas 70% in *R. jostii* and *Amycolatopsis* sp. are predicted to be secreted (*SI Appendix*, Tables S9–S11). Moreover, a larger number of lignin-induced proteins in the exoproteome of *P. putida* lignin cultures is predicted to participate in catabolic (32 to 37 proteins) and biosynthetic processes (74 to 89 proteins) compared with *R. jostii* (10 to 16 and 25 to 33 proteins, respectively) and *Amycolatopsis* sp. (5 to 13 and 20 to 40 proteins, respectively) (*SI Appendix*, Figs. S10–S12). Interestingly, some enzymes from the βKA pathway (considered to be cytoplasmic) were detected in the extracellular fraction of *P. putida* and *R. jostii* in lignin cultures and to a lesser extent, in *Amycolatopsis* sp. (*SI Appendix*, *Text* S2 and Figs. S13–S18 show detailed trends in both intracellular and extracellular fractions for the βKA pathway and alternative routes for the catabolism of aromatics). Taken together, these results highlight the importance of considering other enzyme secretion mechanisms that cannot be predicted by these algorithms or explained due to cell lysis.

Based on these results, we performed electron microscopy to investigate cell integrity and the response to the lignin-rich substrate. Interestingly, we observed that *P. putida* secretes a striking amount of OMVs in lignin-rich media (Fig. 2 *A* and *B*), especially when compared with *P. putida* in lignin-free media or *R. jostii* and *Amycolatopsis* sp. in either media (*SI Appendix*, Fig. S19). In view of these observations, we hypothesized that some of the proteins not predicted to be secreted could be trafficked to the extracellular

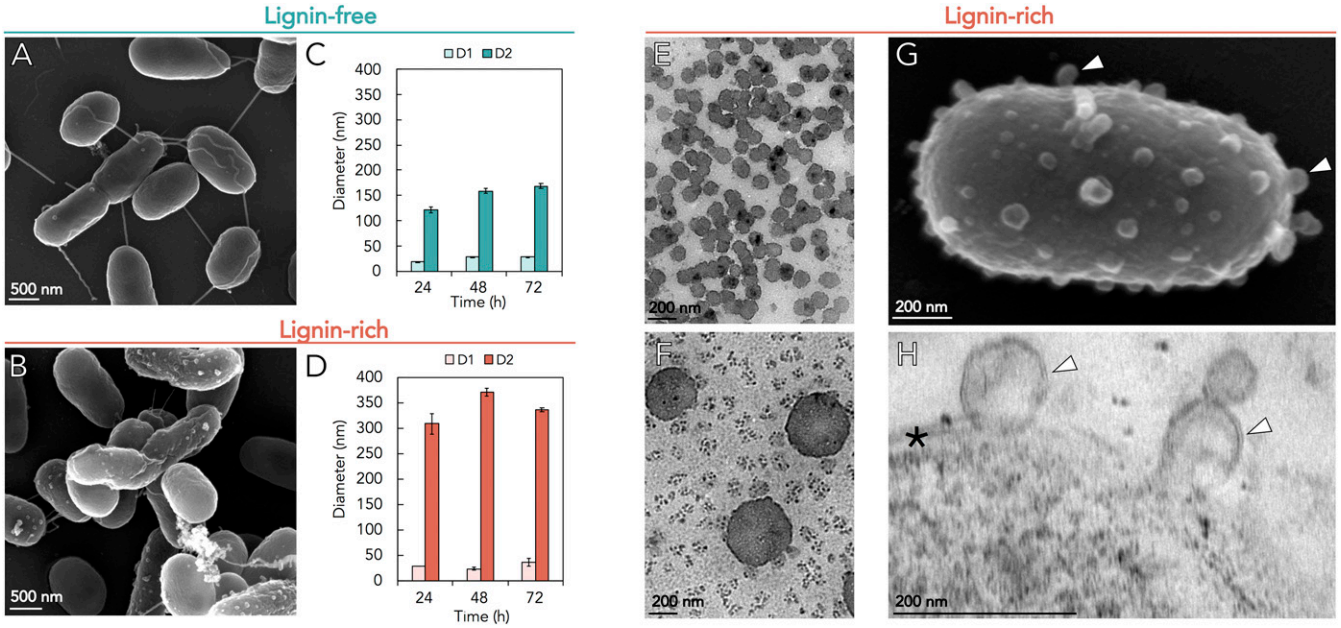

Fig. 2. *P. putida* secretes OMVs of two distinct sizes in lignin-rich media. Representative SEM images of *P. putida* cultivations at 72 h in (*A*) lignin-free and (*B*) lignin-rich media. Diameter of vesicles from *P. putida* cultivations in (*C*) lignin-free and (*D*) lignin-rich media as measured by DLS (intensity). Diameter is reported as an average ± SD of 3 biological replicates and 10 technical replicates for two distributions (D1 and D2), which represent two vesicle subpopulations. (*E* and *F*) TEM images of the two size populations of OMVs from *P. putida* cultivations in lignin-rich media at 72 h. Vesicles were drop cast and stained prior to imaging. (*G*) SEM image of a single *P. putida* with vesicles blebbing (white arrows). (*H*) TEM image of a *P. putida* cell with vesicles blebbing (white arrows) from the outer membrane (black asterisk). Cells were cryofixed, embedded, sectioned, and stained prior to imaging.

compartment via OMVs. Thus, we next focused on *P. putida* OMVs. While the production of OMVs by this bacterium has been previously described (44), their interaction with lignin has not yet been reported. Dynamic light scattering (DLS) measurements and transmission electron microscopy (TEM) (Fig. 2 *E* and *F*) identified two distinct sizes of OMVs in both media formulations with no clear trend in vesicle diameter over time (Fig. 2 *C* and *D*). A 7% increase in cell death is observed in lignin-rich media compared with lignin-free media (*SI Appendix*, Fig. S20), which may contribute to production of vesicles via explosive cell lysis (17). Regardless, both scanning electron microscopy (SEM) and TEM data confirm that OMVs are also secreted via blebbing events from the outer membrane of *P. putida* cells with undamaged membranes even in late stationary phase (Fig. 2 *G* and *H*).

To gain insight into extracellular protein sorting in *P. putida*, the exoproteome was separated into an OMV fraction and the vesicle-free secretome (VFS) (Fig. 3*A*) at 24, 48, and 72 h of cultivation in lignin-free and lignin-rich media and analyzed by proteomics. This timeframe was selected because 1) most changes in the exoproteome were observed (Fig. 1*I*) and 2) oligomeric lignin was the primary carbon source. A rich dataset was generated exhibiting excellent reproducibility between biological triplicates with protein abundance differences driven by fraction, media composition, and time of harvest (*SI Appendix*, Fig. S21 and Dataset S2). In lignin-free media, 50% of the proteins (382 proteins) are differentially abundant between OMV and VFS fractions, from which 58% are enriched in OMVs and 42% are enriched in VFS (Fig. 3*B*). However, during cultivation in lignin-rich media, the number of proteins with differential abundance between fractions increased up to 70% (486 proteins), from which 51% are enriched in OMVs and 49% are enriched in VFS (Fig. 3*B*). Between lignin-rich and lignin-free OMVs, only 32% of the protein cargo are shared (Fig. 3*B*). Of the proteins enriched in OMVs in lignin-free media, only 1% (four proteins) change in abundance across 72 h of cultivation (Fig. 3*B*). Remarkably, growth in lignin-rich media triggers a highly dynamic OMV proteome, with 54% of OMV cargo (263 proteins) changing in abundance across the 72-h cultivation (Fig. 3*B*). Together, OMVs from lignin-rich cultivations exhibit 125 proteins with both lignin-dependent spatial enrichment and temporal changes (*SI Appendix*, Table S12).

Of the OMV proteins that change over time in lignin-rich media, clusters of temporal trends highlight distinct patterns of protein sorting between the OMV fraction and the VFS (Fig. 3*C* and *SI Appendix*, Fig. S22 and Table S13). A pairwise comparison of OMVs in lignin-rich media between 24 and 48 h, between 48 and 72 h, and between 24 and 72 h identified 58, 2, and 236 proteins, respectively, with changing abundance (adjusted *P* value ≤ 0.05) (*SI Appendix*, Fig. S22 and Table S14). Oxidoreductases increase in abundance in the OMVs from 24 to 48 h (Fig. 3*D* and *SI Appendix*, Table S14), corresponding to the shift from catabolism of monomers to interaction with oligomeric lignin in stationary phase. These results corroborate and refine the earlier findings. For example, the first proteomics dataset identified an flavin mononucleotide (FMN)-dependent nicotinamide adenine dinucleotide (NADH)-azoreductase and a quercetin 2,3-dioxygenase to be dynamically enriched in the exoproteome (Fig. 1*I*); here, we refine spatial localization to the OMV and temporal sorting to between 24 and 48 h (Fig. 3*D*). The low (or below the limit of detection) abundance of these proteins in the VFS, even at 72 h of cultivation, suggests that enrichment into vesicles is not an artifact of cell lysis and/or that proteolysis in the VFS occurs rapidly (Fig. 3*D* and *SI Appendix*, Fig. S23).

Surprisingly, many lipoproteins and outer membrane porins (OMPs)—which were originally hypothesized to be constitutive elements of the vesicles—exhibit differential abundance between OMVs in lignin-rich relative to lignin-free media (Fig. 3*E* and *SI Appendix*, Fig. S24). Presence in the VFS under both media conditions precludes the possibility that differences in gene expression underlie this observation (Fig. 3*E*) and thus suggests that these membrane-bound or membrane-associated proteins are selectively excluded from OMV blebbing sites when lignin is

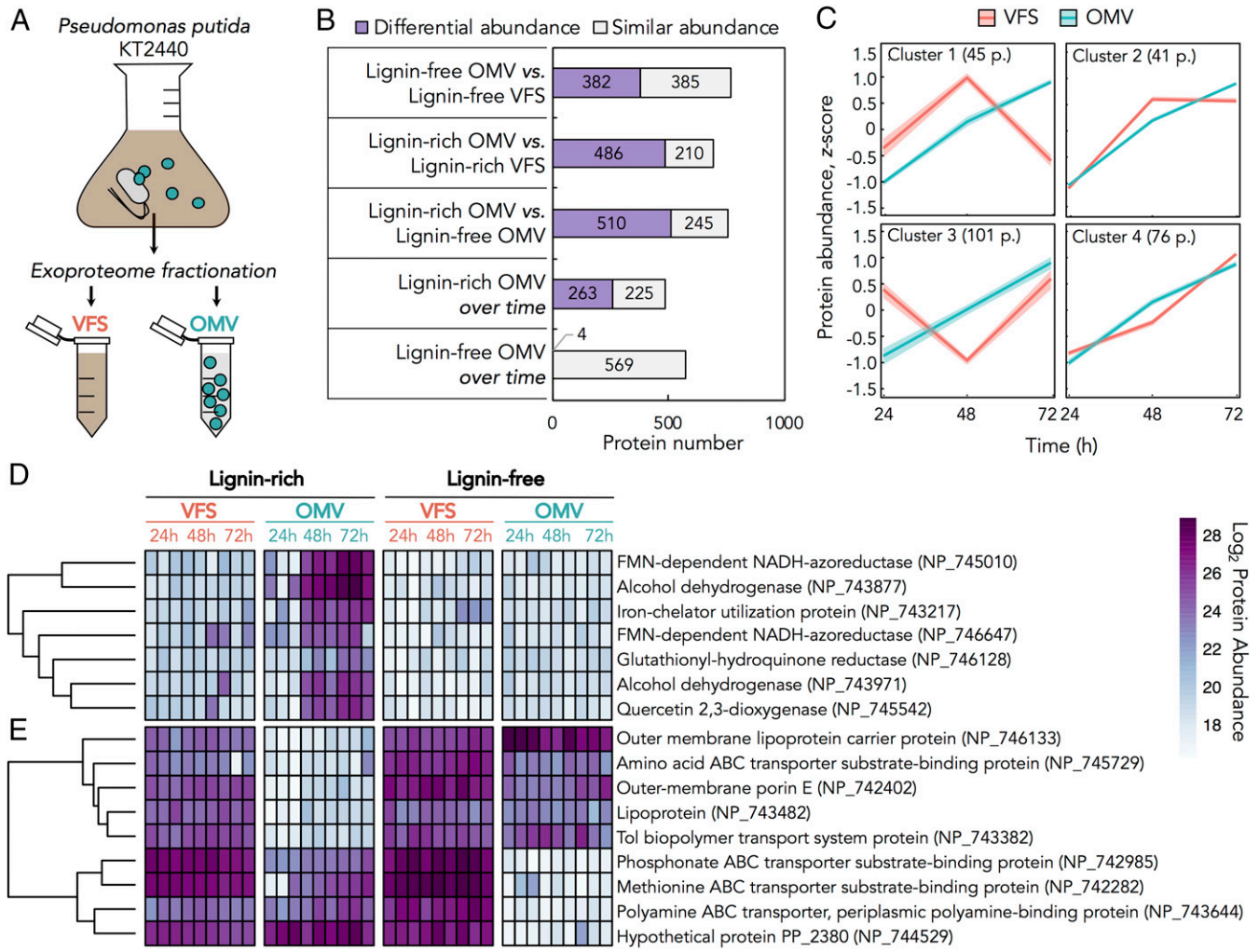

Fig. 3. The exoproteome is selectively compartmentalized into OMVs, and the protein content of OMVs from lignin-rich cultivations is highly dynamic over time. (*A*) The extracellular milieu (= exoproteome) was fractionated into OMVs and VFS prior to proteomics analysis of each fraction from biological triplicates grown in lignin-rich and lignin-free media at 24, 48, and 72 h of cultivation. (*B*) Proteins with differential abundance between the OMV and VFS or OMV over time. Tests were conducted with a pairwise ANOVA on data from biological triplicates, and a Benjamini–Hochberg correction was performed on the resulting *P* values; proteins that had a *P* value < 0.05 are considered to have differential abundance, and those that did not meet this significance cutoff are considered to have similar abundance. Proteins with differential abundance between each time point in lignin-rich OMVs are presented in *SI Appendix*, Table S14. (*C*) Temporal trends of abundance in the OMV and VFS for the 263 proteins (p.) that change over time in lignin-rich OMVs. Clusters were identified by *k*-means clustering, and protein abundance is presented as a *z* score. Trend lines represent the 95% CI for VFS proteins (red) and OMV proteins (blue) in each cluster. The numbers of proteins in each cluster are presented in the upper left-hand corner and listed individually in *SI Appendix*, Table S13. (*D* and *E*) Heat-mapped $\log_2$ protein abundance for select proteins for each biological triplicate at 24, 48, and 72 h of cultivation in the VFS and OMV in lignin-rich and lignin-free media. National Center for Biotechnology Information (NCBI) RefSeq identifiers are provided for each protein in parentheses following the description. (*D*) Select proteins with enrichment into lignin-rich OMVs and function (known or putative) in oxidation–reduction processes. (*E*) Select proteins with differential abundance between lignin-rich and lignin-free OMVs and function (known or putative) as a lipoprotein, small molecular binding protein, transport related, or OMP.

present. Selective exclusion of canonical outer membrane proteins from the OMV has been previously reported (45) but is not widely described. Lipoproteins, OMPs, and lipopolysaccharides are involved in models for selective packaging of cargo and subsequent vesicle biogenesis (46), making these attractive candidates for studying lignin-specific vesiculation and cargo sorting into OMVs.

Next, we examined enzymes from the βKA pathway (Fig. 4*A*) as they were detected in previous exoproteome analysis (*SI Appendix*, Fig. S14). Of the detected proteins in the βKA pathway, all are strongly enriched in the OMVs from lignin-rich media compared with the VFS and the lignin-free exoproteome (Fig. 4*B*). Intra-OMV abundance of βKA enzymes increases temporally after 24 h of cultivation (Fig. 4*B*). Since enrichment is not observed in the VFS, we posit that enzymes in the βKA pathway are secreted via OMVs for the extracellular turnover of lignin-derived aromatics.

To test this hypothesis, we engineered two *P. putida* deletion mutants that cannot grow on two catabolic intermediates: *P. putida* Δ*pobAR* on 4-HBA and *P. putida* Δ*pcaHG* on PCA. These mutants were inoculated to the same cell density and separately complemented with wild-type OMVs for growth analyses (*SI Appendix*, Fig. S25 and Table S15). A boiled OMV control was also included to test if incorporated or encapsulated metabolites (e.g., lipids, amino acids) complement growth. Boiled OMVs enhance growth (measured as optical density at 600 nm [OD_{600}] after 72 h) of *P. putida* Δ*pobAR* by 175% and *P. putida* Δ*pcaHG* by 153% (Fig. 4*C*). Active OMVs enhance growth of *P. putida*

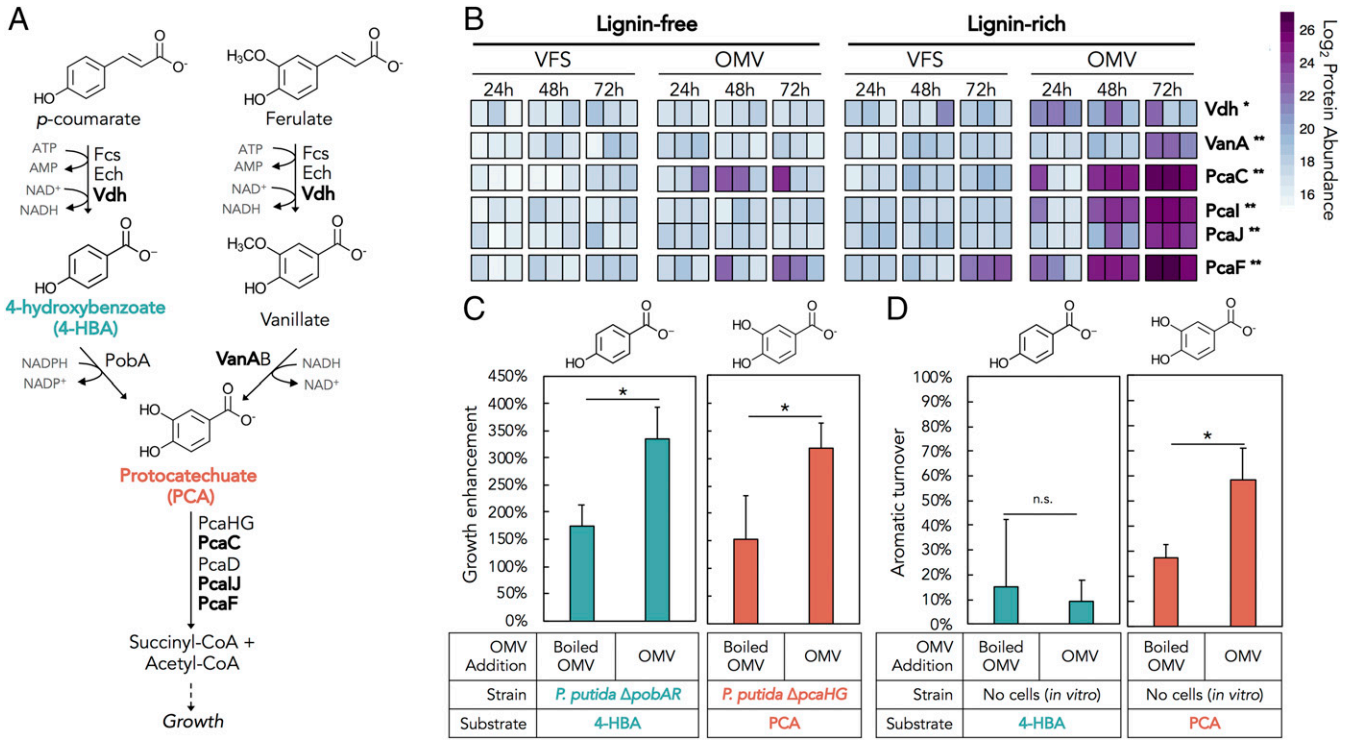

Fig. 4. Catabolism of lignin-derived aromatics via the βKA pathway is enhanced by OMVs. (*A*) The βKA pathway for catabolism of lignin monomers *p*-coumarate and ferulate into succinyl-Coenzyme A (succinyl-CoA) and acetyl-Coenzyme A (acetyl-CoA), which support cellular growth. Metabolites that were used for in vivo and in vitro assays are shown in blue and orange. Proteins in bold were detected in the proteomics analysis. Due to the nontargeted proteomics methodology used throughout this study, we note that lack of detection of certain enzymes from the βKA pathway does not necessarily mean biological absence. (*B*) Proteins detected within the βKA pathway in the VFS or OMV are plotted as a heat map of $\log_2$ abundance. Values for biological triplicate at each time point are plotted separately. $*P < 0.05$ from an ANOVA with Tukey's honest significant difference (HSD) of the VFS relative to OMV; $**P < 0.005$ from an ANOVA with Tukey's HSD of the VFS relative to OMV. (*C*) Improvement of final culture growth (OD_{600}) from complementation of *P. putida* Δ*pobAR* or *P. putida* Δ*pcaHG* with wild-type OMVs (boiled or fresh) for growth on M9 minimal media with 4-HBA or PCA, respectively, as the sole carbon and energy source. Growth enhancement was calculated as the percentage increase in OD_{600} from the mutant strain + substrate to the mutant strain + substrate + OMV. $*P < 0.05$ from a one-tailed paired *t* test. (*D*) In vitro turnover of 4-HBA or PCA by boiled or fresh OMVs. Values are displayed as the percentage decrease in substrate from $t = 0$ h to $t = 24$ h of incubation. n.s., $P > 0.05$ from a one-tailed paired *t* test. $*P < 0.05$ from a one-tailed paired *t* test. Fcs, feruloyl-CoA-synthase; Ech, feruloyl-CoA hydratase-lyase; Vdh, vanillin dehydrogenase; PobA, 4-hydroxybenzoate 3-monooxygenase; VanAB, vanillate O-demethylase; PcaHG, protocatechuate 3,4-dioxygenase; PcaC, 4-carboxymuconolactone decarboxylase; PcaD, 3-oxoadipate enol-lactonase; PcaIJ, 3-oxoadipate CoA-transferase; PcaF, beta-ketoadipyl-CoA thiolase.

Δ*pobAR* cultivations in 4-HBA by 336% and *P. putida* Δ*pcaHG* cultivations in PCA by 319% (Fig. 4*C*). While these growth enhancements are roughly double to what is observed in the boiled control, active OMV complementation does not fully restore the growth observed in wild-type cultivations (*SI Appendix*, Fig. S26 and Table S15), suggesting a limited enzyme content, lifetime in the exoproteome, and/or lack of cofactors.

To further test the hypothesis that OMVs mediate aromatic catabolism, we tested in vitro turnover of 4-HBA and PCA by OMVs. PCA is known to be unstable, which was reflected in the 24 and 27% turnover in abiotic and boiled controls, respectively (Fig. 4*D* and *SI Appendix*, Fig. S27). Interestingly, active OMVs increase the turnover of PCA by 59%, demonstrating that the protocatechuate 3,4-dioxygenase PcaHG remains catalytically active into the OMVs (Fig. 4*D*). Conversely, 4-HBA turnover is not improved by active OMVs (Fig. 4*D*). It is noteworthy that the 4-hydroxybenzoate 3-monooxygenase PobA requires nicotinamide adenine dinucleotide phosphate (NADPH) as a cosubstrate, whereas PcaHG does not (Fig. 4*A*). Considering NAD(P)H instability, its content in isolated OMVs remains unknown. In fact, when OMVs were provided exogenous reducing equivalents, NAD(P)H only decreased in the presence of 4-HBA (*SI Appendix*, Fig. S28). While this does not provide information on the in vivo presence of NAD(P)H or the generation thereof, these results indicate that PobA activity is retained inside the OMV. Together, these data demonstrate that OMV-encapsulated enzymes actively contribute to the turnover of model lignin-derived aromatic compounds.

Discussion

The discovery of extracellular compartmentalization of aromatic–catabolic and putatively ligninolytic enzymes provides insights into microbial lignin conversion. In 2015, we observed that the three bacteria (among 15) studied in this work were top performers in terms of lignin conversion (7). Using these three bacteria, here we quantify the fraction of oligomeric lignin that is utilized, propose that lignin breakdown occurs via β-O-4 bond cleavage based on 2D-HSQC-NMR spectroscopy, and highlight a variety of oxidoreductases and other proteins from exoproteomics data that are worthy of further study to understand bacterial lignin catabolism. Furthermore, we report the spatial subcompartmentalization and temporal dynamics of the exoproteome in *P. putida*, underscoring the importance of considering OMVs to understand bacteria–lignin interactions. In the case of *P. putida*, OMV production has been previously reported to be a response to various environmental stressors and showed media-dependent protein cargo (44, 47, 48). Our results expand on these previous studies by demonstrating temporal cargo sorting of relevant enzymes into OMVs to enhance the extracellular catabolism of lignin-derived aromatic compounds.

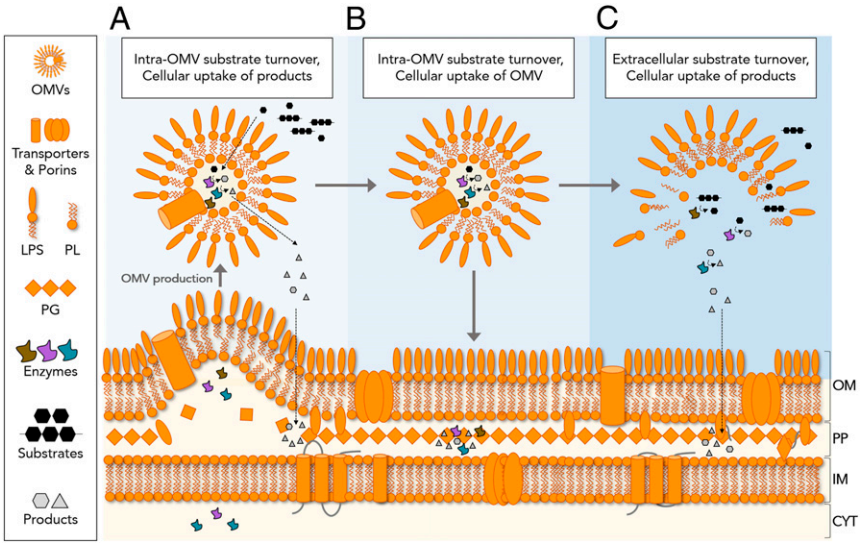

Fig. 5. Model for OMV-mediated nutrient acquisition and/or catabolism of toxic substrates in *P. putida*. A functional set of enzymes is secreted to the extracellular milieu via OMVs in response to a nutrient source, such as lignin-derived compounds. Substrates can then be catabolized inside OMVs, which may require active uptake. Cellular access to the resulting products could then occur via (*A*) uptake of free products released from the OMV or (*B*) direct uptake of OMVs, which would contain encapsulated products. (*C*) Alternatively, secreted vesicles could lyse and release the enzyme mixture into the extracellular milieu for direct access to large substrates, such as lignin. In this scenario, uptake of products would occur as in *A*. CYT, cytoplasm; IM, inner membrane; LPS, lipopolysaccharide; OM, outer membrane; PG, peptidoglycan; PL, phospholipid; PP, periplasm.

Based on this work, we propose a model for OMV-mediated lignin conversion and nutrient acquisition (Fig. 5). In this model, OMVs are first secreted with an encapsulated, functional set of proteins. Substrate turnover could then occur intra-OMV to enable protected enzyme activity and/or cofactor maintenance followed by cellular uptake of released products (Fig. 5*A*) or OMV delivery to the cell (Fig. 5*B*) as has been previously reported (49, 50). Alternatively, the OMV may lyse to allow direct enzymatic access to large substrates and extracellular substrate turnover followed by product uptake by the cell (Fig. 5*C*).

A key limitation of the current study is that we demonstrate functional OMV assays only for aromatic monomers but not for lignin oligomers. While the model presented in Fig. 5 serves to explain the results obtained with monomeric lignin-derived compounds, it could also be applicable to the degradation of oligomeric lignin (Fig. 5*C*). Among others, a challenge to test this model with lignin oligomers and polymers is the difficulty of attributing lignin depolymerization exclusively to enzymes since abiotic processes can also be involved (51). Additionally, cofactor presence and regeneration in OMVs, which would be a requirement for sustained conversion of aromatic compounds and lignin oligomers, also remains challenging to study. Namely, the detection and tracking of unstable compounds, such as NAD(P)H and adenosine triphosphate (ATP), are currently hindered by OMV isolation conditions.

To test and refine the model in Fig. 5, additional studies are required to interrogate OMV lifetime, metabolite import and export from OMVs, and OMV–cell fusion events. An important outstanding question relates to the extent of extracellular carbon turnover by the OMVs relative to intracellular turnover. To address this question, spatially resolved fluxomics, which was recently developed and applied to exosomes (52, 53), and quantitative proteomics of the βKA pathway, will be key to understanding the spatial distribution of aromatic catabolism (extracellular vs. intracellular) in vivo. Another interesting observation from the current study is the size heterogeneity of OMVs, which potentially suggests functional specialization and different routes for OMV biogenesis. Recent work using asymmetric flow field flow fractionation to separate vesicles by size discovered distinct protein and lipid profiles attributed to exosome subpopulations (54), revealing a layer of complexity that remains to be explored in bacterial OMVs.

This work demonstrates that OMVs harbor functional aromatic–catabolic enzymes, but the evolutionary and physiological driver for use of OMVs in this context remains unknown. OMV production may benefit *P. putida* KT2440 and other bacteria that deploy OMVs by providing a means to access nutrient sources that cannot translocate the cell membrane and/or mitigate substrate toxicity (both intrinsic and generated through metabolic intermediates) (55) by restricting cytoplasmic encounters or by modifying toxic compounds to less toxic molecules extracellularly, thus increasing strain fitness. *P. putida* KT2440 is derived from *P. putida* mt-2, which is studied for its remarkable capability to degrade toluene and other toxic pollutants (56, 57). The general metabolic versatility (58) and robust toxicity tolerance (22, 59) attributed to Pseudomonads have inspired widespread adoption of domesticated *P. putida* for biotechnology and bioremediation (60, 61). Future exploration of the role of OMVs in *P. putida* KT2440 may serve to provide direct insights into how OMVs contribute to microbial robustness in toxic environments.

Going forward, OMV-mediated secretion of biological components for extracellular biocatalysis can also be considered as a synthetic biology tool. Engineered packaging of specific enzymes into OMVs has been demonstrated via bioconjugation to OmpA (62). Protein scaffolding is an interesting possibility for OMV-mediated secretion of functional sets of enzymes, both as a means to explain the natural phenomena of coordinated protein secretion in the absence of identifiable secretion tags and as an engineering tool (63). Encapsulation and secretion of enzymes via OMVs could also serve to protect cargo from proteolysis (64), enable long-distance delivery of proteins or other biological materials (65), enhance the tolerance for the utilization or production of toxic compounds of interest in engineered strains, and promote extracellular digestion of complex substrates (66–68). Overall, the current work shows that focus is needed to understand how OMVs are used in carbon cycling and for conversion of waste organic carbon into valuable chemical products as well as to exploit bacterial OMVs for biotechnological applications.

Methods

A brief materials and methods section is presented here. *SI Appendix, SI Methods* has further details.

Bacterial Cultivations. *P. putida* KT2440 (ATCC 47054), *R. jostii* RHA1 (provided by Lindsay Eltis, the University of British Columbia, Vancouver, BC, Canada), and *Amycolatopsis* sp. (ATCC 39116) were inoculated at an OD_{600} of 0.1 in M9 minimal media with 5 g/L glucose (lignin-free cultivations) and incubated at 30 °C and 225 rpm. Lignin-rich cultivations contained the same media plus additional 25% (vol/vol) soluble alkaline lignin from corn stover (prepared as previously described) (55).

Cell Viability Analyses. Samples from *P. putida* cultivations were diluted in Tris-buffered saline and stained with LIVE/DEAD BacLight (Invitrogen; L7012) per the manufacturer's instructions, and fluorescence was measured with 525/540 and 610/620 bandpass filters on a CytoFLEX flow cytometer (Beckman Coulter Life Sci.). Percentages of live and dead cells were calculated after appropriate gating.

Strain Engineering in *P. putida* KT2440. The genetically modified *P. putida* KT2440 strains utilized in this work, Δ*pcaHG* (=CJ072) and Δ*pobAR* (=CJ182), were constructed as described previously (69).

OMV Characterization.

OMV isolation. OMV enrichment was prepared from 0.2 μm vacuum filter-clarified *P. putida* KT2440 supernatant using the ExoBacteria kit (SBI; #EXOBAC100A) ion exchange protocol following the manufacturer's instructions.

DLS analyses. Enriched OMVs were analyzed in a Dyna Pro Plate Reader (Wyatt) by detecting scattered photons at 158°. The hydrodynamic diameter was calculated by fitting the autocorrelation function with medium refraction index of 1.33 and medium viscosity of 1.019 cp.

SEM. Samples from bacterial cultivations were plated on poly-L-lysine–coated glass coverslips, fixed with glutaraldehyde, dehydrated in increasing concentrations of ethanol, critical point dried, coated in Ir, mounted, and imaged with an FEI Quanta 400 FED SEM under 0.45 torr and beam accelerating voltage of 30 keV.

TEM. Enriched OMVs were drop cast onto a glow-discharged carbon film 200-mesh copper grid and stained. *P. putida* cultivations were preserved with high-pressure freeze substitution, embedded, sectioned, and stained. Images were acquired with a 4-megapixel Gatan UltraScan 1000 camera on an FEI Tecnai G2 20 Twin 200 kV LaB6.

OMV Assays.

OMV complementation assays. OMVs were enriched from *P. putida* KT2440 lignin-rich cultivations at 72 h. An aliquot of OMVs was heated to 100 °C for >1 h and used as a boiled control. OMVs were added to washed *P. putida* Δ*pcaHG* or *P. putida* Δ*pobAR* cultivations in M9 minimal media with 10 mM protocatechuic acid or 10 mM 4-hydroxybenzoic acid, respectively, and incubated at 30 °C and 225 rpm. Colony forming units (CFUs) were measured on Lysogeny Broth agar plates. OD_{600} was measured using an FLUOstar Omega plate reader.

OMV in vitro assays. OMVs were enriched from *P. putida* lignin-rich cultivations at 72 h, ultracentrifuged at 150,000 × *g* to pellet vesicles, resuspended in phosphate-buffered saline (PBS), and incubated with 2 mM protocatechuic acid or 2 mM 4-hydroxybenzoic acid at 30 °C and 225 rpm. Samples for metabolite analysis were quantified by LC-MS/MS.

NAD(P)H Consumption Assays. OMVs were enriched from *P. putida* lignin-rich cultivations at 72 h, proteins were extracted, and absorbance at 340 nm was measured in the presence of a combination of 1 mM 4-HBA (pH 7.0), 250 μM NADH, and/or 250 μM NADPH immediately after addition of proteins for 600 s.

Lignin and Metabolite Analyses.

Gel permeation chromatography. Gel permeation chromatography of soluble alkaline lignin from corn stover was conducted as previously described for lignin molecular weight analysis (26).

Compositional analysis. The bacterial supernatants from lignin-rich medium were freeze dried, and lignin content was analyzed as previously described (70).

2D-HSQC-NMR. The bacterial supernatants from lignin-rich medium were lyophilized, ball milled, suspended in d6-DMSO/d5 pyridine (4:1, vol/vol), and sonicated, and spectra were acquired on a Bruker Avance III 600-MHz spectrometer at 11.7 T using a triple resonance inverse (TCI) cryoprobe.

Metabolite quantification: Aromatic compounds, glucose, and carboxylic acids. Aromatic compounds in the lignin-rich supernatant were analyzed by electrospray ionization (ESI) LC-MS/MS on an Ion Trap SL (Agilent) as previously described (26). Glucose and small acids in the culture supernatants were analyzed by LC refractive index detector/ultraviolet absorbance (UV) on a Agilent 1200 LC system as previously described (71). Aromatic compounds in the OMV in vitro assays were analyzed by ESI-LC-MS/MS on a 6470 Triple Quadrupole Mass Spectrometer (Agilent) with multiple reaction monitoring for each analyte.

Proteomics Analyses.

Intracellular and extracellular proteomics in the three bacterial species. Samples from bacterial cultivations were fractionated into cell pellets and supernatants, processed, and flash frozen. Proteins were denatured, concentrated, extracted with chloroform:methanol as previously described (72), dried, denatured, digested with trypsin, and desalted. Peptides were detected on a Velos Pro Orbitrap Mass Spectrometer (ThermoScientific). MS/MS data search, peptide quantitation, and data analysis are detailed in *SI Appendix*.

OMV and VFS proteomics from* P. putida *KT2440. Supernatants from bacterial cultivations were fractionated in OMV and VFS using the ExoBacteria kit, flash frozen, concentrated, washed, denatured, extracted with chloroform:methanol:water, dried, digested with trypsin, and desalted. Peptides were detected on a Q Exactive Plus Mass Spectrometer. MS/MS data search, peptide quantitation, and data analysis are detailed in *SI Appendix*.

Data Availability. Proteomics data from *P. putida*, *R. jostii*, and *Amycolatopsis* sp. are available at the MassIVE database (accession no. MSV000084524) and the ProteomeXchange database (accession no. PXD016114) (73). Proteomics data from *P. putida* OMV and VFS are available at the MassIVE database (accession no. MSV000084506) (74).

ACKNOWLEDGMENTS. This work was authored in part by Alliance for Sustainable Energy, LLC, the manager and operator of the National Renewable Energy Laboratory for the US Department of Energy (DOE) under Contract DE-AC36-08GO28308. Funding for the time-resolved exoproteomics efforts was provided by the US DOE, Office of Energy Efficiency and Renewable Energy, Bioenergy Technologies Office. The isolation and proteomics study of the OMVs and OMV assays were funded by The Center for Bioenergy Innovation, a US DOE Bioenergy Research Center supported by the Office of Biological and Environmental Research in the DOE Office of Science. The exoproteomics of the three bacteria was done at the Environmental Molecular Sciences Laboratory (EMSL) (grid.436923.9), a DOE Office of Science User Facility sponsored by the Office of Biological and Environmental Research. Portions of the microscopy and light scattering work were supported in part by Laboratory Directed Research and Development funding from Argonne National Laboratory provided by the Director, Office of Science, of the US DOE under Contract DE-AC02-06CH11357. Use of the Center for Nanoscale Materials, an Office of Science user facility, was supported by the US DOE, Office of Science, Basic Energy Sciences, under the same contract. We thank Christopher W. Johnson and Payal Khanna for sharing the *P. putida* deletion strains. We thank Darren Peterson and David Brandner for providing the alkaline pretreated lignin liquor. We thank Samantha Peters and Payal Chirania for their assistance in proteomic sample preparation at Oak Ridge National Laboratory (ORNL). We thank Adam Guss for providing materials and laboratory space to conduct part of this work at ORNL. We thank Gregory A. Tira for support of initial *P. putida* OMV characterization experiments at Argonne National Laboratory. We thank Therese Clauss and Rosey Chu at EMSL for help with the proteomics measurements.

1. D. Floudas *et al.*, The Paleozoic origin of enzymatic lignin decomposition reconstructed from 31 fungal genomes. *Science* **336**, 1715–1719 (2012).
2. W. Boerjan, J. Ralph, M. Baucher, Lignin biosynthesis. *Annu. Rev. Plant Biol.* **54**, 519–546 (2003).
3. A. T. Martínez *et al.*, Biodegradation of lignocellulosics: Microbial, chemical, and enzymatic aspects of the fungal attack of lignin. *Int. Microbiol.* **8**, 195–204 (2005).
4. E. Masai, Y. Katayama, M. Fukuda, Genetic and biochemical investigations on bacterial catabolic pathways for lignin-derived aromatic compounds. *Biosci. Biotechnol. Biochem.* **71**, 1–15 (2007).
5. T. D. Bugg, M. Ahmad, E. M. Hardiman, R. Rahmanpour, Pathways for degradation of lignin in bacteria and fungi. *Nat. Prod. Rep.* **28**, 1883–1896 (2011).
6. N. Kamimura *et al.*, Bacterial catabolism of lignin-derived aromatics: New findings in a recent decade: Update on bacterial lignin catabolism. *Environ. Microbiol. Rep.* **9**, 679–705 (2017).
7. D. Salvachúa, E. M. Karp, C. T. Nimlos, D. R. Vardon, G. T. Beckham, Towards lignin consolidated bioprocessing: Simultaneous lignin depolymerization and product generation by bacteria. *Green Chem.* **17**, 4951–4967 (2015).
8. G. Fuchs, M. Boll, J. Heider, Microbial degradation of aromatic compounds—from one strategy to four. *Nat. Rev. Microbiol.* **9**, 803–816 (2011).

9. A. J. Ragauskas *et al.*, Lignin valorization: Improving lignin processing in the biorefinery. *Science* **344**, 1246843 (2014).
10. T. D. H. Bugg, R. Rahmanpour, Enzymatic conversion of lignin into renewable chemicals. *Curr. Opin. Chem. Biol.* **29**, 10–17 (2015).
11. G. T. Beckham, C. W. Johnson, E. M. Karp, D. Salvachúa, D. R. Vardon, Opportunities and challenges in biological lignin valorization. *Curr. Opin. Biotechnol.* **42**, 40–53 (2016).
12. J. Becker, C. Wittmann, A field of dreams: Lignin valorization into chemicals, materials, fuels, and health-care products. *Biotechnol. Adv.* **37**, 107360 (2019).
13. J. V. Vermaas *et al.*, Passive membrane transport of lignin-related compounds. *Proc. Natl. Acad. Sci. U.S.A.* **116**, 23117–23123 (2019).
14. L. Lin *et al.*, Systems biology-guided biodesign of consolidated lignin conversion. *Green Chem.* **18**, 5536–5547 (2016).
15. X. Li *et al.*, Discovery of potential pathways for biological conversion of poplar wood into lipids by co-fermentation of *Rhodococci* strains. *Biotechnol. Biofuels* **12**, 60 (2019).
16. M. Kumar *et al.*, Genomic and proteomic analysis of lignin degrading and polyhydroxyalkanoate accumulating β-proteobacterium *Pandoraea* sp. ISTKB. *Biotechnol. Biofuels* **11**, 154 (2018).
17. C. Schwechheimer, M. J. Kuehn, Outer-membrane vesicles from Gram-negative bacteria: Biogenesis and functions. *Nat. Rev. Microbiol.* **13**, 605–619 (2015).
18. L. Brown, J. M. Wolf, R. Prados-Rosales, A. Casadevall, Through the wall: Extracellular vesicles in gram-positive bacteria, mycobacteria and fungi. *Nat. Rev. Microbiol.* **13**, 620–630 (2015).
19. A. T. Jan, Outer Membrane vesicles (OMVs) of gram-negative bacteria: A perspective update. *Front. Microbiol.* **8**, 1053 (2017).
20. M. Toyofuku, N. Nomura, L. Eberl, Types and origins of bacterial membrane vesicles. *Nat. Rev. Microbiol.* **17**, 13–24 (2019).
21. C. S. Harwood, R. E. Parales, The beta-ketoadipate pathway and the biology of self-identity. *Annu. Rev. Microbiol.* **50**, 553–590 (1996).
22. M. Chavarría, P. I. Nikel, D. Pérez-Pantoja, V. de Lorenzo, The Entner-Doudoroff pathway empowers *Pseudomonas putida* KT2440 with a high tolerance to oxidative stress. *Environ. Microbiol.* **15**, 1772–1785 (2013).
23. W. Lan *et al.*, Elucidating tricin-lignin structures: Assigning correlations in HSQC spectra of monocot lignins. *Polymers (Basel)* **10**, 916 (2018).
24. S. D. Mansfield, H. Kim, F. Lu, J. Ralph, Whole plant cell wall characterization using solution-state 2D NMR. *Nat. Protoc.* **7**, 1579–1589 (2012).
25. A. Das *et al.*, Lignin conversion to low-molecular-weight aromatics via an aerobic oxidation-hydrolysis sequence: Comparison of different lignin sources. *ACS Sustain. Chem. Eng.* **6**, 3367–3374 (2018).
26. D. Salvachúa *et al.*, Lignin depolymerization by fungal secretomes and a microbial sink. *Green Chem.* **18**, 6046–6062 (2016).
27. J. Rencoret *et al.*, A commercial laccase-mediator system to delignify and improve saccharification of the fast-growing *Paulownia fortunei* (Seem.) Hemsl. *Holzforschung* **73**, 45–54 (2018).
28. M. Ahmad *et al.*, Identification of DypB from *Rhodococcus jostii* RHA1 as a lignin peroxidase. *Biochemistry* **50**, 5096–5107 (2011).
29. A. Santos, S. Mendes, V. Brissos, L. O. Martins, New dye-decolorizing peroxidases from *Bacillus subtilis* and *Pseudomonas putida* MET94: Towards biotechnological applications. *Appl. Microbiol. Biotechnol.* **98**, 2053–2065 (2014).
30. M. E. Brown, T. Barros, M. C. Chang, Identification and characterization of a multifunctional dye peroxidase from a lignin-reactive bacterium. *ACS Chem. Biol.* **7**, 2074–2081 (2012).
31. R. S. Granja-Travez, T. D. H. Bugg, Characterization of multicopper oxidase CopA from *Pseudomonas putida* KT2440 and *Pseudomonas fluorescens* Pf-5: Involvement in bacterial lignin oxidation. *Arch. Biochem. Biophys.* **660**, 97–107 (2018).
32. S. Majumdar *et al.*, Roles of small laccases from *Streptomyces* in lignin degradation. *Biochemistry* **53**, 4047–4058 (2014).
33. S. A. Misal, K. R. Gawai, Azoreductase: A key player of xenobiotic metabolism. *Bioresour. Bioprocess.* **5**, 17 (2018).
34. A. M. Gonçalves, S. Mendes, D. de Sanctis, L. O. Martins, I. Bento, The crystal structure of *Pseudomonas putida* azoreductase - the active site revisited. *FEBS J.* **280**, 6643–6657 (2013).
35. J. J. P. Griese, R. P Jakob, S. Schwarzinger, H. Dobbek, Xenobiotic reductase A in the degradation of quinoline by *Pseudomonas putida* 86: Physiological function, structure and mechanism of 8-hydroxycoumarin reduction. *J. Mol. Biol.* **361**, 140–152 (2006).
36. T. Widiatningrum, S. Maeda, K. Kataoka, T. Sakurai, A pirin-like protein from *Pseudomonas stutzeri* and its quercetinase activity. *Biochem. Biophys. Rep.* **3**, 144–149 (2015).
37. P. I. Lario, N. Sampson, A. Vrielink, Sub-atomic resolution crystal structure of cholesterol oxidase: What atomic resolution crystallography reveals about enzyme mechanism and the role of the FAD cofactor in redox activity. *J. Mol. Biol.* **326**, 1635–1650 (2003).
38. A. Greule, J. E. Stok, J. J. De Voss, M. J. Cryle, Unrivalled diversity: The many roles and reactions of bacterial cytochromes P450 in secondary metabolism. *Nat. Prod. Rep.* **35**, 757–791 (2018).
39. A. T. Martínez *et al.*, Oxidoreductases on their way to industrial biotransformations. *Biotechnol. Adv.* **35**, 815–831 (2017).
40. J. D. Bendtsen, H. Nielsen, D. Widdick, T. Palmer, S. Brunak, Prediction of twin-arginine signal peptides. *BMC Bioinformatics* **6**, 167 (2005).
41. T. N. Petersen, S. Brunak, G. von Heijne, H. Nielsen, SignalP 4.0: Discriminating signal peptides from transmembrane regions. *Nat. Methods* **8**, 785–786 (2011).
42. J. D. Bendtsen, L. Kiemer, A. Fausbøll, S. Brunak, Non-classical protein secretion in bacteria. *BMC Microbiol.* **5**, 58 (2005).
43. N. Y. Yu *et al.*, PSORTb 3.0: Improved protein subcellular localization prediction with refined localization subcategories and predictive capabilities for all prokaryotes. *Bioinformatics* **26**, 1608–1615 (2010).
44. C. W. Choi *et al.*, Proteomic characterization of the outer membrane vesicle of *Pseudomonas putida* KT2440. *J. Proteome Res.* **13**, 4298–4309 (2014).
45. K. J. McMahon, M. E. Castelli, E. García Vescovi, M. F. Feldman, Biogenesis of outer membrane vesicles in *Serratia marcescens* is thermoregulated and can be induced by activation of the Rcs phosphorelay system. *J. Bacteriol.* **194**, 3241–3249 (2012).
46. K. E. Bonnington, M. J. Kuehn, Protein selection and export via outer membrane vesicles. *Biochim. Biophys. Acta* **1843**, 1612–1619 (2014).
47. T. Baumgarten *et al.*, Membrane vesicle formation as a multiple-stress response mechanism enhances *Pseudomonas putida* DOT-T1E cell surface hydrophobicity and biofilm formation. *Appl. Environ. Microbiol.* **78**, 6217–6224 (2012).
48. R. Marisa Heredia *et al.*, Release of outer membrane vesicles in *Pseudomonas putida* as a response to stress caused by cationic surfactants. *Microbiology* **162**, 813–822 (2016).
49. Y. Tashiro *et al.*, Interaction of bacterial membrane vesicles with specific species and their potential for delivery to target cells. *Front. Microbiol.* **8**, 571 (2017).
50. E. J. O'Donoghue, A. M. Krachler, Mechanisms of outer membrane vesicle entry into host cells. *Cell. Microbiol.* **18**, 1508–1517 (2016).
51. V. Gómez-Toribio, A. B. García-Martín, M. J. Martínez, Á. T. Martínez, F. Guillén, Induction of extracellular hydroxyl radical production by white-rot fungi through quinone redox cycling. *Appl. Environ. Microbiol.* **75**, 3944–3953 (2009).
52. W. D. Lee, D. Mukha, E. Aizenshtein, T. Shlomi, Spatial-fluxomics provides a subcellular-compartmentalized view of reductive glutamine metabolism in cancer cells. *Nat. Commun.* **10**, 1351 (2019).
53. A. Achreja *et al.*, Exo-MFA - A 13C metabolic flux analysis framework to dissect tumor microenvironment-secreted exosome contributions towards cancer cell metabolism. *Metab. Eng.* **43**, 156–172 (2017).
54. H. Zhang *et al.*, Identification of distinct nanoparticles and subsets of extracellular vesicles by asymmetric flow field-flow fractionation. *Nat. Cell Biol.* **20**, 332–343 (2018).
55. D. Salvachúa *et al.*, Bioprocess development for muconic acid production from aromatic compounds and lignin. *Green Chem.* **20**, 5007–5019 (2018).
56. E. Belda *et al.*, The revisited genome of *Pseudomonas putida* KT2440 enlightens its value as a robust metabolic chassis. *Environ. Microbiol.* **18**, 3403–3424 (2016).
57. P. I. Nikel, V. de Lorenzo, *Pseudomonas putida* as a functional chassis for industrial biocatalysis: From native biochemistry to trans-metabolism. *Metab. Eng.* **50**, 142–155 (2018).
58. P. H. Clarke, The metabolic versatility of pseudomonads. *Antonie van Leeuwenhoek* **48**, 105–130 (1982).
59. P. Calero *et al.*, Genome-wide identification of tolerance mechanisms toward *p*-coumaric acid in *Pseudomonas putida*. *Biotechnol. Bioeng.* **115**, 762–774 (2018).
60. P. Dvořák, P. I. Nikel, J. Damborský, V. de Lorenzo, Bioremediation 3.0: Engineering pollutant-removing bacteria in the times of systemic biology. *Biotechnol. Adv.* **35**, 845–866 (2017).
61. P. I. Nikel, E. Martínez-García, V. de Lorenzo, Biotechnological domestication of pseudomonads using synthetic biology. *Nat. Rev. Microbiol.* **12**, 368–379 (2014).
62. N. J. Alves *et al.*, Bacterial Nanobioreactors–Directing enzyme packaging into bacterial outer membrane vesicles. *ACS Appl. Mater. Interfaces* **7**, 24963–24972 (2015).
63. J. B. Y. H. Behrendorff, G. Borràs-Gas, M. Pribil, Synthetic protein scaffolding at biological membranes. *Trends Biotechnol.*, S0167-7799(19)30250-1 (2019).
64. N. J. Alves, K. B. Turner, I. L. Medintz, S. A. Walper, Protecting enzymatic function through directed packaging into bacterial outer membrane vesicles. *Sci. Rep.* **6**, 24866 (2016).
65. J. M. Bomberger *et al.*, Long-distance delivery of bacterial virulence factors by *Pseudomonas aeruginosa* outer membrane vesicles. *PLoS Pathog.* **5**, e1000382 (2009).
66. R. G. de Paula *et al.*, Extracellular vesicles carry cellulases in the industrial fungus *Trichoderma reesei*. *Biotechnol. Biofuels* **12**, 146 (2019).
67. M. Ø. Arntzen, A. Várnai, R. I. Mackie, V. G. H. Eijsink, P. B. Pope, Outer membrane vesicles from *Fibrobacter succinogenes* S85 contain an array of carbohydrate-active enzymes with versatile polysaccharide-degrading capacity. *Environ. Microbiol.* **19**, 2701–2714 (2017).
68. S. Ichikawa *et al.*, Cellulosomes localise on the surface of membrane vesicles from the cellulolytic bacterium *Clostridium thermocellum*. *FEMS Microbiol. Lett.* **366**, fnz145 (2019).
69. R. K. Jha *et al.*, A protocatechuate biosensor for *Pseudomonas putida* KT2440 via promoter and protein evolution. *Metab. Eng. Commun.* **6**, 33–38 (2018).
70. J. B. Sluiter *et al.*, Compositional analysis of lignocellulosic feedstocks. 1. Review and description of methods. *J Agric. Food Chem.* **58**, 9043–9053 (2010).
71. E. M. Karp *et al.*, Post-fermentation recovery of biobased carboxylic acids. *ACS Sustain. Chem. Eng.* **6**, 15273–15283 (2018).
72. D. Wessel, U. I. Flügge, A method for the quantitative recovery of protein in dilute solution in the presence of detergents and lipids. *Anal. Biochem.* **138**, 141–143 (1984).
73. D. Salvachúa *et al.*, Outer membrane vesicles catabolize lignin-derived aromatic compounds in *Pseudomonas putida* KT2440. MassIVE. https://massive.ucsd.edu/ProteoSAFe/dataset.jsp?task=1641318954204d098df29fd731c9384b. Deposited 1 November 2019.
74. D. Salvachúa *et al.*, Outer membrane vesicles catabolize lignin-derived aromatic compounds in *Pseudomonas putida* KT2440. MassIVE. https://massive.ucsd.edu/ProteoSAFe/dataset.jsp?task=5bb4ad4ae04d47119e4fc9fb158fd389. Deposited 25 October 2019.